PHDS Co.
3011 Amherst Road
Knoxville, TN 37921
www.phdsco.com

Principal Investigator:
Matthew Kiser, Ph.D.
Director of Physics
PHDS Co.

Phase I Final Technical Report: High-Resolution Gamma-ray Imaging and Spectroscopy for Special Nuclear Material Assay (GeGI-DNN)

Phase I Grant Award Number: DE-SC0013734

Phase I Summary

The Phase I program focused on the development, implementation, and evaluation of spectral and spatial algorithms to improve the intrinsic image quality and efficiency of GeGI-DNN for count-starved (low activity) measurement scenarios. As a direct result of the Phase-I achievements, Pinhole imaging efficiency was dramatically improved, Compton imaging performance was improved by incorporating a statistical treatment of the Compton image, and quantitative image analysis routines were developed and implemented. The following bullet points describe the Phase I activities:

- A GeGI was made available to the Phase I program. This GeGI was used during multiple measurements of SNM at Oak Ridge National Laboratory, as well as at a Technology Demonstration Workshop (TDW) on Gamma Imaging hosted by the International Atomic Energy Agency in Seibersdorf, Austria (IAEA 2015).
- The GeGI Imager32 software application was modified to produce output data streams compatible with Stabilization/Render Safe (JTOT) analysis tools. Imager32 now readily exports spectra in the ANSI/IEEE standard N42.42 format, and the GeGI detector response function has been defined and tested using GADRAS-DRF. Additionally, the "Reachback" button in Imager32 can now send an email directly from the unit containing data for analysis by DOE Triage.
- A statistical treatment of the spherical Compton image was developed and implemented within Imager32. The user may now select a threshold of interest for displaying the centroid of the Compton image distribution that corresponds to the number of sigma above background ($N\sigma$) in the Compton spatial distribution.
- Waveform-decomposition algorithms exercised on a 140-mm detector motivated a change to the baseline detector strip-pattern design to be used for the GeGI-DNN prototype design.
- Quantitative imaging analysis routines were developed for both Pinhole and Compton imaging modalities. *This is a major milestone making GeGI-DNN the first truly quantitative spectroscopic imaging system.*
- Pinhole imaging performance was improved by implementing spectral-statistical peak search on a pixel-by-pixel basis, integrating Compton events into the pinhole image reconstruction, varying the pinhole aperture size, and developing a pinhole plug for background measurement and subtraction.

- The front-end electronics were modified to increase the gamma-ray energy range from 3 MeV to 12 MeV full scale to measure high-energy gamma rays from neutron capture reactions in surrounding materials.
- A new GeGI-DNN system design was created to accommodate DNN missions. The new system design leverages the new compact PHDS SPECT32-HR electronics and a low-power mechanical cooler.

Modification of the GeGI Imager32 Software Application for Ease of Use in DNN Missions

Several DNN missions require detector operation in weapons-related facilities, where security constraints are significant. To facilitate ease of entry and setup portability for GeGI-DNN, the Imager32 software application was modified to require minimal administrative access on the Windows computer used to operate the system. During Phase II, the Imager32 software will move completely away from using the Windows Registry. USB driver installation is currently the only step of Imager32 installation and operation that requires administrative access, so such access is only required during the initial install (a one-time action).

The Imager32 software application was also modified to produce output data streams compatible with Stabilization/Render Safe (JTOT) analysis tools. Imager32 now exports ANSI/IEEE N42.42 spectral files formatted to be processed in analysis tools routinely employed by the DNN community such as Peak Easy, Gamma Designer, Cambio, and GADRAS. Furthermore, the "Reachback" button in Imager32 can now send an email directly from the GeGI tablet/laptop (assuming a network connection is available) to any email address, such as DOE Triage. The email attachments include a summary report of the measurement parameters and results, the Imager32 file containing the spectral and image information, and the N42 spectrum file for the full detector.

As proof-of-concept that GeGI-DNN will provide data of use to the DNN community, the project PI obtained a Single User Software License for the GADRAS-DRF software package from the Radiation Safety Information Computational Center (RSICC) at ORNL. Using GADRAS-DRF, a detector response file (DRF) was generated for the GeGI detector with data collected from several sources of known activity positioned at a fixed distance. The GeGI DRF was then applied to multiple data files to extract the identity and quantity of material present. An example analysis is shown in Figure 1 – the spectral information from a GeGI Compton image was exported to the N42 file, which was then analyzed by GADRAS-DRF. As shown, ^{137}Cs and ^{133}Ba were located with Compton imaging in Imager32; analysis of the N42 file associated with this data in GADRAS-DRF indicates 8.9 μCi of ^{137}Cs and 18.5 μCi of ^{133}Ba, which is correct to within the uncertainty of the measurement. GADRAS-DRF also spectrally identified the ^{57}Co source that was located behind the detector.

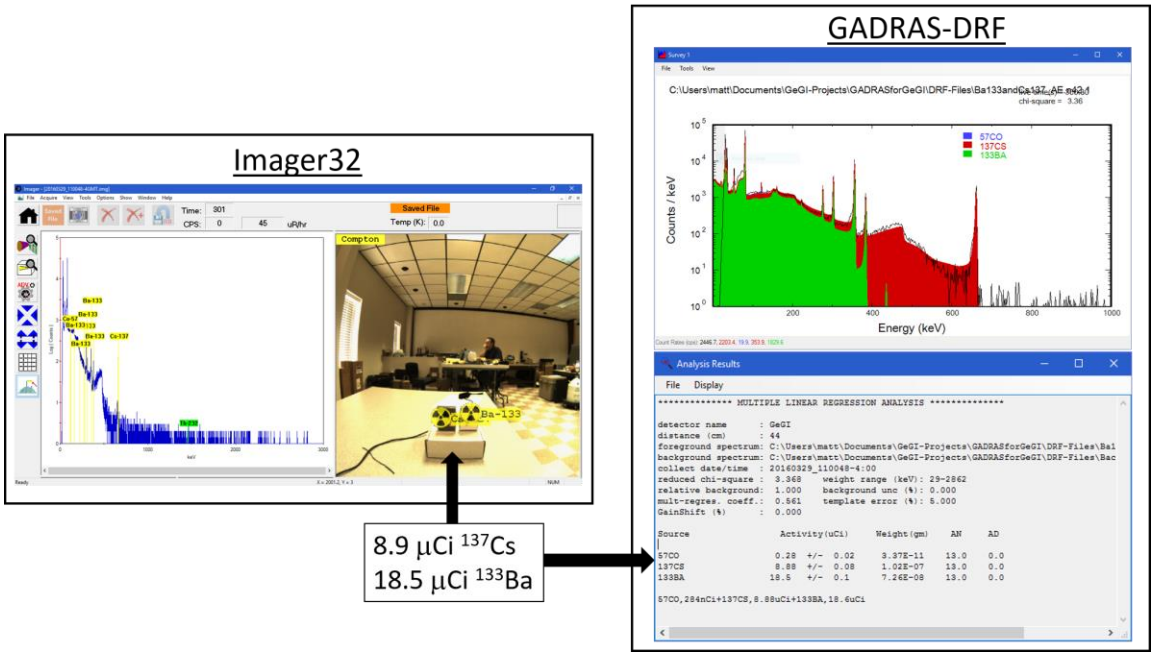

Figure 1: A DRF was generated for the full GeGI detector. The N42 file exported from the Compton image in Imager32 (left) was ingested by GADRAS-DRF and analyzed using the GeGI DRF. GADRAS-DRF indicated 8.9 µCi of ^{137}Cs and 18.5 µCi of ^{133}Ba, which is within the uncertainty of the measurement. GADRAS-DRF also detected and calculated an activity for ^{57}Co, but this analysis is not accurate because the ^{57}Co was located behind the detector.

Quantitative Analysis Methods for Compton and Pinhole Images

One of the most significant achievements of Phase I was the development and implementation of real-time, on-line quantitative analysis for both Compton and Pinhole imaging. These calculations incorporate the detection efficiency as a function of energy and the spatial response of the detector for the Compton and Pinhole imaging modes. As is generally the case for quantitative analysis of gamma-ray spectra, the most significant contributions to the uncertainty are those parameters related to the source term, namely distance to the source, intervening material(s), and self-attenuation. Each of these parameters (and the associated uncertainties) have been considered and may be entered by the user in the Imager32 software interface to yield the best possible quantitative analysis.

The quantitative imaging analyses are fundamentally driven by the spectral detection and identification algorithms within Imager32. A peak-search algorithm runs at user-defined time intervals to detect and highlight statistically significant gamma-ray photopeaks in the energy spectrum. A follow-on identification algorithm then determines the likely isotope and categorizes the material as SNM, Industrial, Medical, or Naturally Occurring Radioactive Material (NORM) – the identification library currently includes the 37 most common and important isotopes including those pertinent to SNM. Once identified, the yield (or branching ratio) of the gamma-ray of interest is known, thus enabling quantitative analysis. Alternatively, the user may also manually select a gamma-ray of interest from a library of over 400 isotopes containing a total of ~25,000 gamma rays.

For Compton imaging, the quantitative analysis provides a conservative upper limit for the amount of activity present for each isotope of interest. The energy spectroscopy and angular information from the Compton image are analyzed together to calculate the activity (quantity) of each isotope identified and located within the forward 2π field of view. Source activities are not calculated in the rear 2π field of the Compton image because intervening materials within the GeGI system cause variable attenuation. An example quantitative Compton image of a barrel encountered during a live CBRNE exercise is shown in Figure 2. Note that the 3 mm thick steel drum material has been added as intervening material for the quantitative analysis, as well as a distance and distance uncertainty for error propagation.

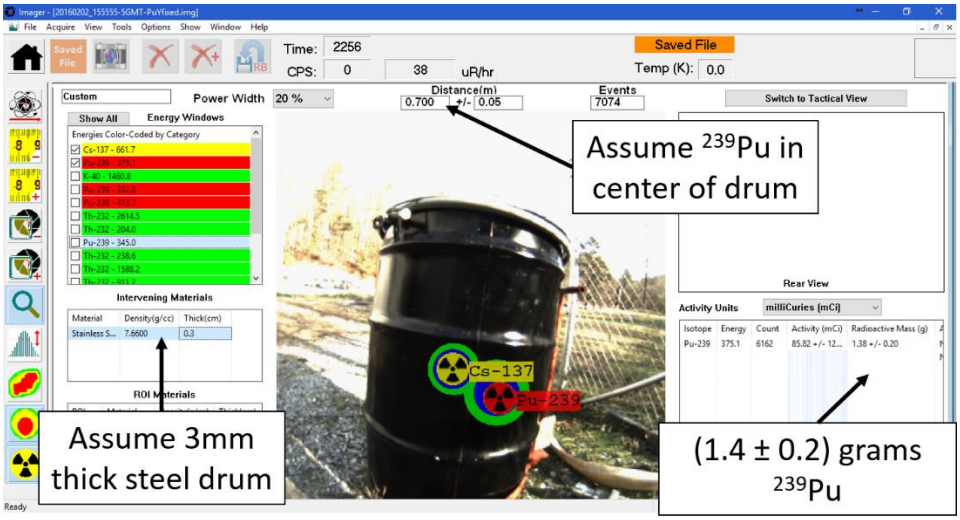

Figure 2: Quantitative analysis of a Compton image of a drum encountered during a CBRNE exercise. The GeGI-DNN quantitative analysis algorithm developed and implemented during Phase I calculated 1.4 grams of ^{239}Pu in the barrel. This matches the actual mass (1.4 grams) within the propagated error. A separate analysis (not shown) of the ^{137}Cs signature using 2.5 cm of intervening Pb (the source was in a Pb pig) indicates 500 μCi of ^{137}Cs.

For Pinhole imaging, the detector response as a function of energy and angle within the 60° field of view is used to calculate the activity/mass of any isotopes of interest. Pinhole imaging is a direct back-projection of the radioactivity distribution. As such, the Pinhole image itself may be analyzed to calculate the absolute radioactivity/mass of any number and/or shape of objects within the field of view. During Phase I, analysis of the Pinhole image was incorporated into Imager32, allowing the user to select regions in the image for which to calculate the source activity. Any arbitrary shape can be selected by simply tracing the desired shape around the particular region of apparent activity. Imager32 automatically calculates the quantity of all isotopes in that region. In addition, an apparent background region can be selected to determine whether the activity in each region is statistically significant. Quantitative analysis of the Pinhole image of a triangular distribution encountered during a CBRNE exercise is shown in Figure 3. This analysis clearly demonstrates the power of quantitative pinhole imaging. The ^{239}Pu triangle was measured to be remarkably uniform throughout the individual compartments of the triangular object – this measurement is the first of its kind to quantitatively assess the interior ^{239}Pu distribution of this special-forms object.

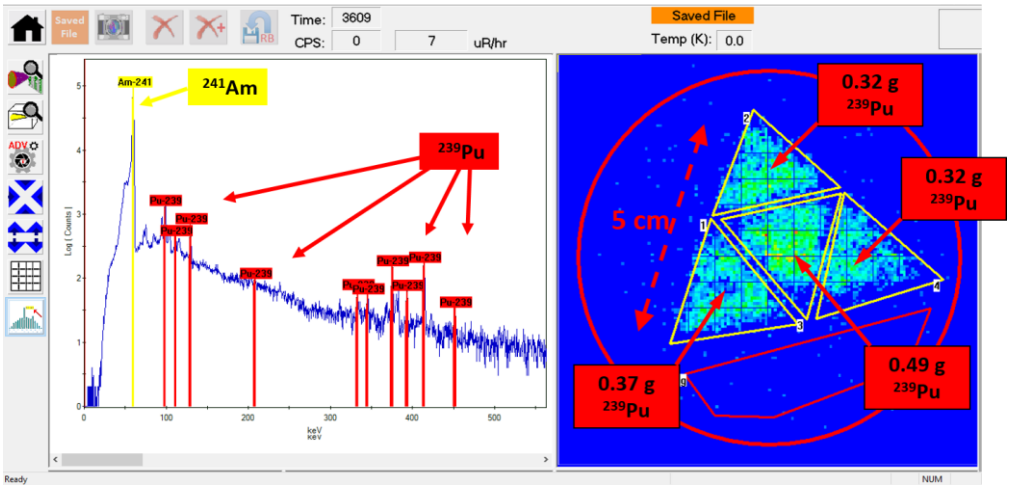

Figure 3: Quantitative analysis of the Pinhole image from Error! Reference source not found.**. The small triangular compartments of the larger triangular object were found to have a reasonably uniform distribution of ^{239}Pu, quantified to range from 0.32 grams to 0.49 grams. The total mass was calculated to be (1.5 ± 0.2) grams, which is consistent with the known mass of 1.4 grams.**

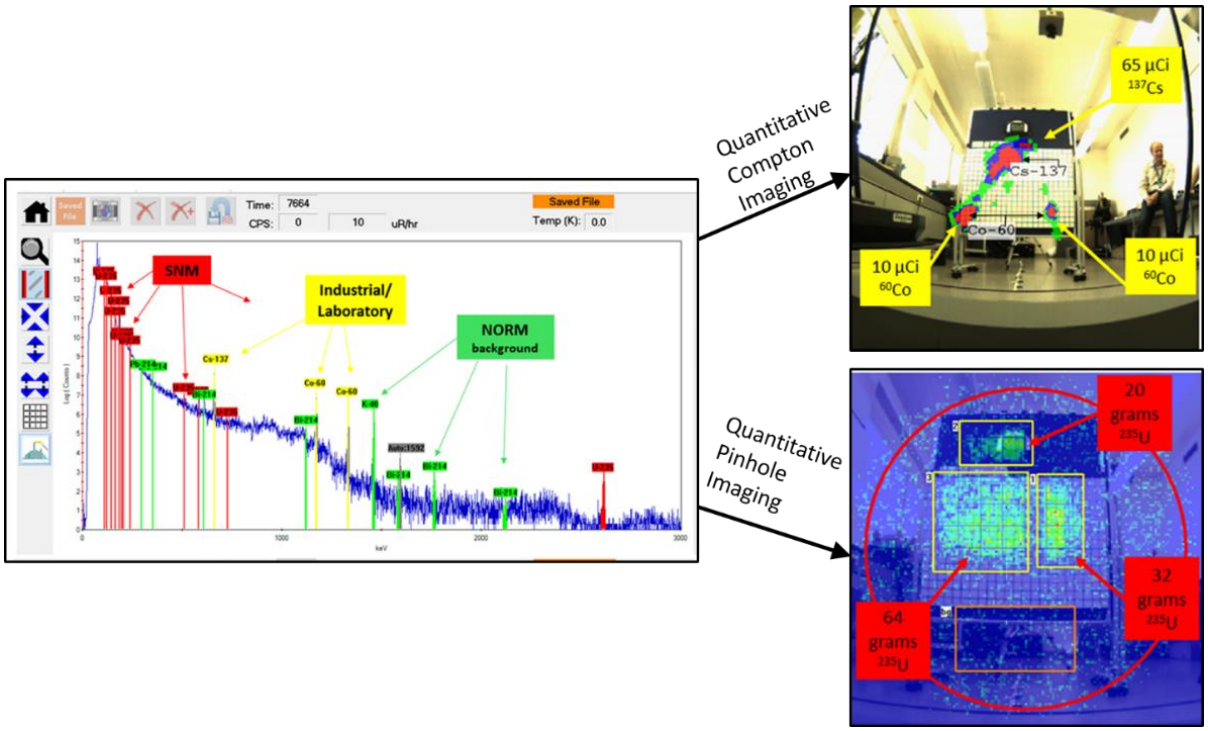

Figure 4: Simultaneous quantitative Compton and Pinhole images collected against a source distribution at the IAEA TDW in Austria (IAEA 2015). Analysis of the Compton image indicates 65 µCi of ^{137}Cs and two locations of ^{60}Co of about 10 µCi each. Analysis of the selected regions of interest in the Pinhole image (indicated by the yellow rectangles) calculates a total of ~116 grams of ^{235}U distributed as shown.

Quantitative Compton and Pinhole images may also be measured simultaneously, as was demonstrated at the IAEA TDW on Gamma Imaging in Seibersdorf, Austria (IAEA 2015) during Phase I of this project. At the TDW, unknown source configurations were arranged on the back of a screen such that the GeGI operator was not aware of the particular isotopes and geometries. Data

were then collected and analyzed by GeGI in real time to detect, identify, locate, and quantify the sources within the field of view. An example of a simultaneous Compton/Pinhole image is shown in Figure 4 – note that the Compton image clearly resolved ^{137}Cs and ^{60}Co sources while the Pinhole image measured three distinct distributions of ^{235}U. Analysis of the Compton image (accounting for the 2.54 cm thick pinhole shield) indicates 65 μCi of ^{137}Cs and two locations of ^{60}Co of about 10 μCi each. Analysis of the selected regions of interest in the Pinhole image indicates about 116 grams of ^{235}U contained in three distinct regions of the image. The GeGI-DNN quantitative image processing allowed all of this information to be obtained with a single measurement from a single standoff position 2.5 meters from the target. PHDS personnel operating the GeGI had no *a priori* knowledge of the source configuration during these measurements. During all of the TDW measurements, the sensitivity, resolution and quantification of the GeGI made it the most outstanding instrument at the workshop, by a substantial margin.

Compton Gamma-ray Imaging Advances

During Phase I, a 3-dimensional peak detection algorithm was developed to determine the location and degree of localization of a radioactive source based purely on an automated statistical analysis of the spherical Compton-image space. This imaging improvement was inspired by statistical alarming algorithm work done by our LLNL collaborator, Dr. Morgan Burks, as part of his ongoing NA-22 work (Kiser, et al. 2014). Due to the random overlap of the Compton-kinematic acceptance rings on the 4π spherical image, the centroid (peak) of the raw Compton image distribution can move about randomly and inconsistently when the statistics are poor (as shown in the left of Figure 5). To provide an objective means by which to determine true source location, a statistical detection threshold is set by the user in the Compton imaging space. The algorithm then calculates the volume under the Compton peak, which is then compared with the root-mean-square (RMS) noise in the full 4π Compton image. The peak strength is computed and compared to the 4π RMS Compton image background to determine the number of standard deviations of the peak above background. The GeGI-DNN Imager32 software allows the user to select a desired threshold number (*N*) of standard deviations above background for spatial detection. An example of the statistical significance of the region around the Compton centroid (as reflected by the number of standard deviations above background) as a function of the number of Compton imaging events (which scales with time) for the 662 keV gamma rays from ^{137}Cs is shown at the right of Figure 5.

It should be noted that the angular bounds used for peak detection in the Compton image is a function of energy and has been parametrized from 136 keV up to 2614 keV. The angular resolution does indeed improve with increasing energy like $\sim\frac{1}{E}$ just as stated by the basic Compton scatter equation. The gamma-ray energy and this statistical factor are now used to prevent the visual suggestion of a statistically-poor source location. No source location is displayed until the Compton image peak is more than *N* standard deviations above background. Generally speaking, we find that reasonably well localized sources converge to a non-misleading location after ~3σ. Of course advanced users can easily override this feature by disabling the Compton image auto-detect and enabling the visual display of the raw Compton image on the optical counterpart.

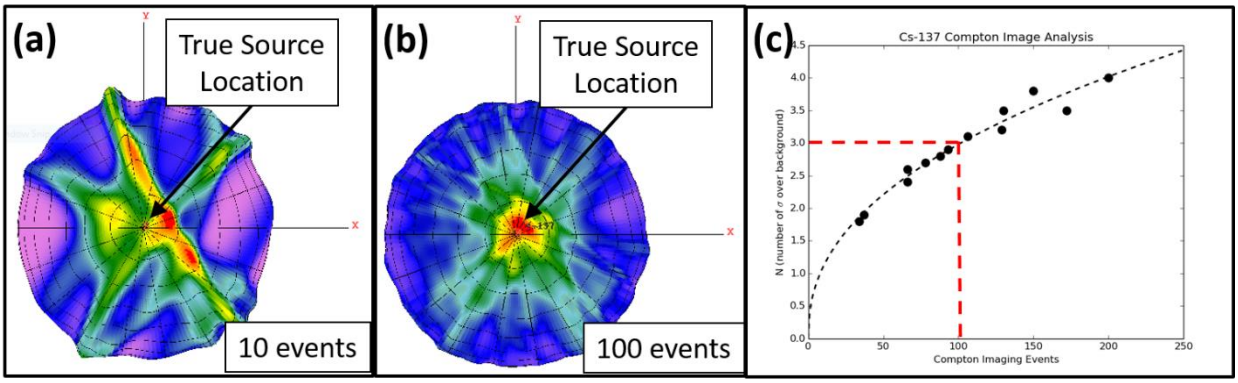

Figure 5: (a) Raw Compton image example for 662-keV gamma rays with low statistics (10 events). When statistics are poor, the location of the peak centroid of this distribution can vary significantly. (b) As statistics improve (in this example, 100 events), the distribution of 662-keV gamma rays in the raw Compton image becomes more focused and the centroid stabilizes. (c) Statistical significance of the Compton source distribution around the centroid as a function of number of Compton imaging events for 662-keV gamma rays. During Phase I, we found that a statistical significance of 3σ corresponds to ~100 Compton events over a relatively broad range of gamma-ray energies.

Decomposition of the raw ADC waveforms for each of the 32 channels of the GeGI detector provides a means by which to increase Compton imaging efficiency by identifying Compton scatter events followed by photoelectric absorption within a single detector pixel. These types of intra-pixel interactions are not discernible with the parametric spatial-interpolation approach currently used in the COTS GeGI. Events occurring within a single pixel are currently treated as single photoelectric-absorption interactions. Phase I included an investigation of waveform decomposition using an existing 140-mm diameter laboratory prototype detector that had been slated as the baseline detector design for the GeGI-DNN prototypes to be fabricated during Phase II. While the waveform-decomposition analysis clearly provides a factor of ~3 improvement in Compton imaging efficiency at 662 keV in the 90-mm detector (16x16 strip; 5 mm strip pitch), the waveform-decomposition analysis *did not function properly* with the 140-mm diameter detector (16x16 strip; 7.75 mm strip pitch) due to an important unforeseen noise problem. The 7.75-mm wide strips of the 140-mm diameter detector have a measured capacitance of ~78 pF each. This capacitance is far enough beyond the 10-pF capacitance of the JFETs in the preamplifiers to cause a non-linear noise increase not previously observed or predicted by the conventional understanding of JFET channel noise (Radeka 1968, Goulding 1972). This noise increase is roughly a factor of ~3 greater than originally anticipated, sufficient to degrade the spatial resolution within the width of the strip to ~6 mm when waveform decomposition is applied to the 7.75 mm wide strips. This means that waveform decomposition is not of substantial advantage in a detector of this particular geometry (strip pitch) with these particular JFETs (preamplifiers).

The source of the anomalous noise was determined to arise from JFET channel noise from any given JFET being capacitively injected into the neighboring strip and preamplifier because of the disparity between the 78-pF strip capacitance and the 10-pF JFET capacitance. We found that mounting 4-6 additional JFETs in parallel on a preamplifier and increasing the drain current appropriately caused the anomalous noise to abate. In principle, multiple JFETs could be tiled together in this manner to decrease this noise-injection susceptibility for each channel sufficiently

to allow waveform decomposition on the 16x16 strip 7.75-mm pitch 140-mm diameter detector to be used in Phase II. Unfortunately, no high-quality (low-noise) n-channel JFETs exist in the world having 60-80 pF of capacitance and a transconductance/capacitance that scales anywhere close to the 10-pF BF862 JFETs we currently use. Tiling multiple BF862 JFETs requires careful drain-current curve matching that does not lend itself to reasonable manufacturing. After weighing the various risks and tradeoffs, the decision was made to decrease the designed strip pitch of the GeGI-DNN prototype detector from 7.75 mm down to 3 mm to decrease the strip capacitance down to ~ 30 pF. This decision increases the number of strips from the 16x16 design to a 42x42 strip array on the 140-mm diameter crystal. Given all of the various tradeoffs, the 3-mm detector pitch was deemed to be the best overall system solution for a successful Phase II GeGI-DNN prototype. This initially frustrating noise discovery was probably the most significant risk-management detail learned from the Phase I project. Since the inherent spatial uncertainty of a gamma-ray within a given strip is 3 mm rather than 7.75 mm to begin with, a 3-mm strip-pitch detector is inherently far less reliant upon waveform decomposition and/or the parametric spatial algorithms. Thanks to significantly more compact electronic processing electronics (like the SPECT32-HR), the relative complexity associated with the addition of more detector channels is now far less difficult to manage as our instrumentation has evolved.

Pinhole Gamma-ray Imaging Advances

One significant Pinhole imaging improvement during Phase I was actually relatively straightforward but effective in improving the flexibility of GeGI-DNN. Originally developed for preclinical nuclear medicine applications, the only pinhole aperture ever used previously with GeGI was a 1-mm diameter 60º pinhole. While the 1-mm diameter pinhole provides excellent spatial resolution, the efficiency can be low in some applications. Phase-I measurements of U_3O_8 reference cylinders at ORNL required long-dwell measurements to acquire sufficient statistics when using the 1-mm pinhole. To address this, 3-mm and 5-mm diameter prototype pinhole apertures (60º acceptance) were constructed during Phase I. As expected, the 3-mm and 5-mm diameter pinholes yield factors of ~9 and ~25 efficiency improvement, scaling with the area of the open pinhole, compared to the 1-mm diameter pinhole. Sample pinhole images of a ^{57}Co source in the far field for a 1-mm and 5-mm pinhole are shown in Figure 6. Development of these three pinhole options during Phase I presents a wide range of flexibility for GeGI-DNN users that may be limited by time constraints or driven by a spatial resolution requirement. Although the larger pinhole apertures necessarily degrade the spatial resolution in the image somewhat, this is often the best tradeoff for making initial measurements. In some cases, distances and source strengths provide only enough counting statistics when using the larger diameter pinholes. For example, the ^{235}U array measurements shown in Figure 4 would not have been possible without the 5 mm pinhole. There was only one opportunity and one time period available to measure this particular scenario at the IAEA TDW – a situation commonly occurring in NNSA DNN measurement campaigns.

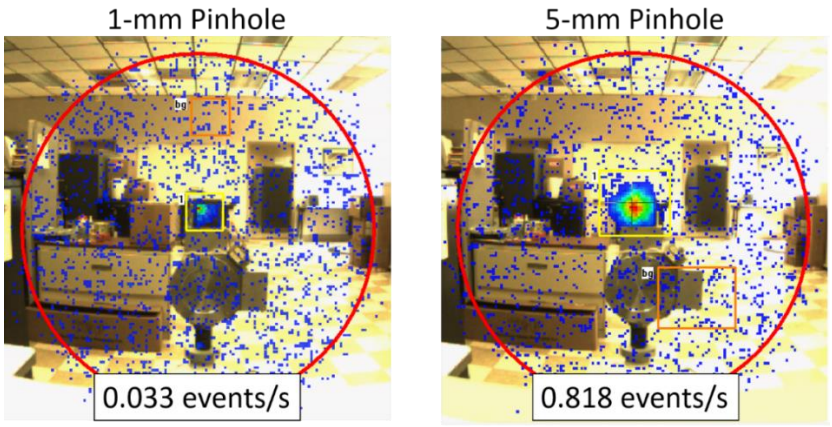

Figure 6: Pinhole images of a ^{57}Co source at a distance of 1.5 meters using 1-mm and 5-mm pinholes. The 5-mm pinhole is ~25 times more efficient than the 1-mm pinhole, with image resolution degraded by a factor of ~3.5.

Another method developed during Phase I to increase Pinhole imaging efficiency integrates Compton events into the Pinhole image in addition to photoelectric-absorption events. Previously, only gamma rays that photoelectrically absorbed upon first interaction in the detector were included in the Pinhole image. These gamma rays generate a single event in the detector, and a simple pinhole back-projection (flipped horizontally and vertically) of this event leads to the Pinhole image (as depicted at the left of Figure 7). Including gamma rays that first Compton scatter then absorb in the detector increases the imaging efficiency – the only challenge is reliably determining the location of the first interaction in the detector, which serves as the event location to be projected onto the Pinhole image (left of Figure 7). The Compton-photoelectric event-sequence determination used by our Compton imaging was integrated into the Pinhole-imaging code for this purpose. The improvement in Pinhole imaging efficiency resulting from the inclusion of Compton events is shown on the right-hand side of Figure 7 as a function of incident gamma-ray energy. For higher energy gamma rays that primarily Compton scatter as the first interaction in the detector, the efficiency improvement approaches a factor of ~2.

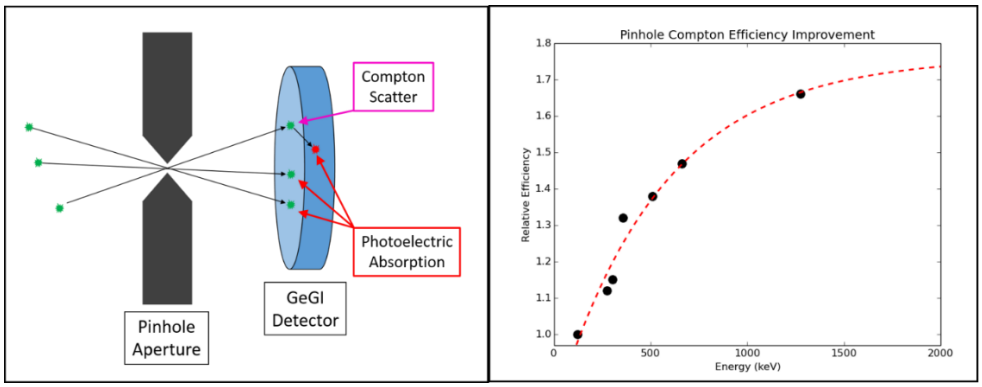

Figure 7: (Left) Diagram of Pinhole imaging of gamma rays of a given energy. Gamma rays that photoelectrically absorb are simply back-projected to form the Pinhole image. For gamma rays that Compton scatter prior to absorption, the sequence of events must be approached probabilistically since timing cannot resolve the interactions. (Right) Plot of Pinhole imaging efficiency improvement resulting from inclusion of Compton-scatter events as a function of incident gamma-ray energy.

Given the complex nature of several measurement environments encountered during the Phase-I period, the concept of a pinhole plug was investigated. By collecting data in a given static situation with the pinhole aperture both open and closed, the most reliable background subtraction can be applied to account for sources outside the field of view and/or gamma-ray leakage through the pinhole shield. During Phase I, 60-degree conical pinhole plugs were manufactured for the GeGI pinhole shields to explore the efficacy of this approach. As expected, the quality of images generated in environments with low signal-to-noise (whether high background or low source signal) were greatly improved by applying the pinhole-plug (pinhole/anti-pinhole) methodology. As shown in Figure 8, a Fiestaware teapot coated with uranium glaze was imaged with a 5-mm pinhole and then again with the pinhole plug inserted. The signal-to-noise of this measurement is quite low, due to the low-level radiation content of the uranium glaze and the relatively small amount of the glaze. While the shape of the teapot is not readily discernible in the Pinhole-Open Image, the Net-Pinhole Image clearly shows the teapot shape. Another example of the pinhole plug concept in a high background environment is depicted in Figure 9. Here a 122 keV source (^{57}Co) is evident in the Pinhole-Open Image, but other features within the 122-keV energy window are also visible. Applying a background subtraction with the Pinhole-Plugged Image results in a very clean (and quantitative) Net-Pinhole Image. The GeGI-DNN pinhole/anti-pinhole measurement technique is ideal for situations where SNM object shape certainty and clarity are at a premium.

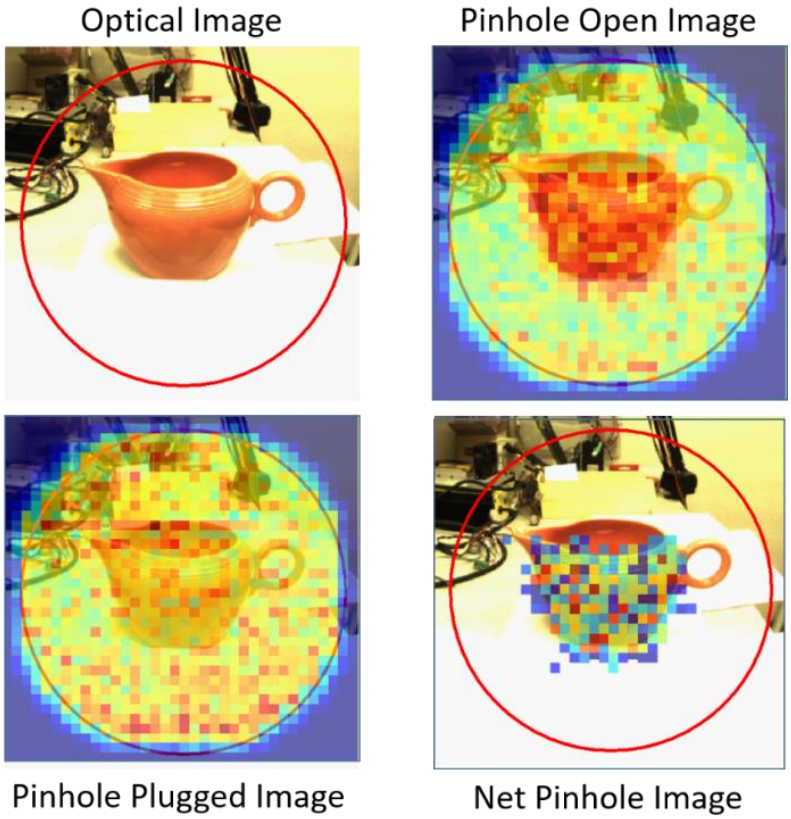

Figure 8: Demonstration of the pinhole plug concept with a uranium-glazed Fiestaware teapot. Data were collected with the 5-mm pinhole aperture both open and closed. The resulting Net Pinhole Image clearly indicates the shape of the teapot.

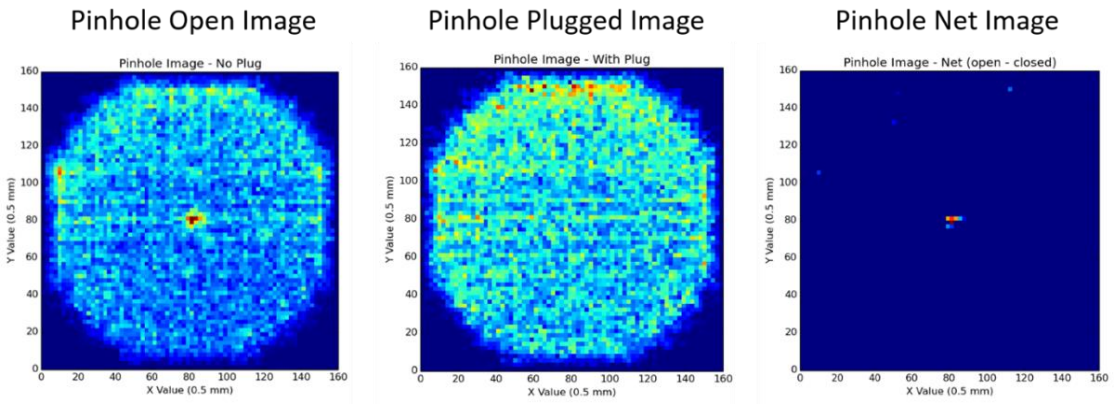

Figure 9: Demonstration of the pinhole plug concept with a point-like source of ^{57}Co in a high background from ^{137}Cs, ^{133}Ba, and ^{60}Co resulting in substantial down-scatter into the 122 keV imaging window. Note that using the Pinhole Plugged Image for background subtraction results in a very clean and unambiguous image of the ^{57}Co source.

Another Pinhole imaging advancement accomplished during Phase I was real-time spectral analysis of the energy-spectrum data on a pixel-by-pixel basis as an objective means by which to detect and identify any statistically significant source regions within the Pinhole image. This was a natural follow-on to the spherical peak-detection algorithm developed for Compton imaging described earlier. Because the spectral signal-to-noise is overwhelmingly greater in regions (pixels) of the pinhole image containing the sources relative to the spectrum from the entire detector, this approach is able to simultaneously detect and locate regions of interest in the Pinhole image significantly more efficiently than a visual analysis alone. Often one cannot actually "see" the source above background but the pixel-spectrum analysis undeniably identifies the actual source region by an overwhelming statistical factor that cannot be misleading. As a proof of concept, a pinhole peak-search algorithm was implemented to analyze spectra for the 16x16 pixels defined by the orthogonal strips of the COTS GeGI detector. An example analysis is shown in Figure 10 for Pinhole imaging of a ^{57}Co point source. The pixel spectra triggered a detection in pixel (23, 8) at a confidence level greater than 6σ (six standard deviations) while the neighboring pixel (23, 9) without view of the source showed only 0.4σ in the 122-keV energy window. The source spot is not visible to the eye in the pinhole image shown in the upper left-hand side of Figure 10.

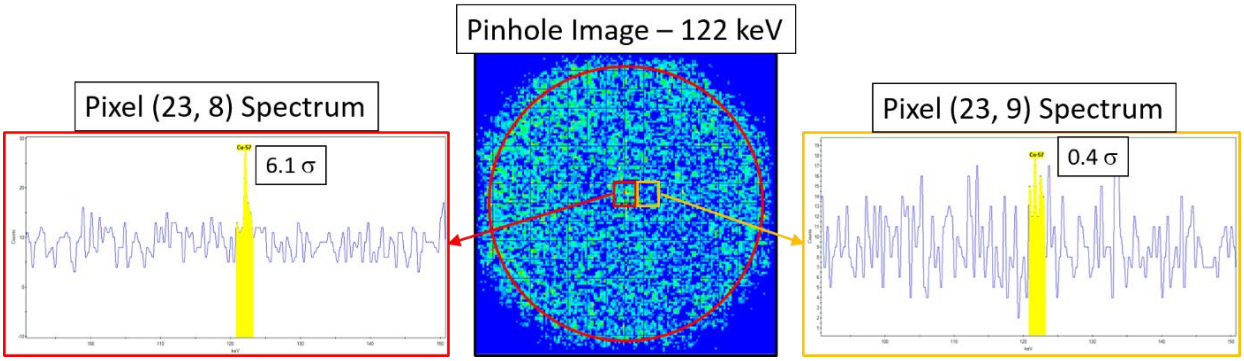

Figure 10: Automated analysis of the spectra associated with regions of the Pinhole image will detect statistically significant sources before they are readily visible in the image. In this example, real-time analysis of the 16x16 pixel spectra resulted in the detection of a 122 keV peak in pixel (23, 8) at greater than 6σ. Analysis of the spectrum from neighboring pixel (23, 9) does not indicate a peak of statistical significance.

GeGI-DNN System Design

The full system design for GeGI-DNN was completed during Phase I with a focus on accommodating DNN missions by providing a large diameter (140-mm) highly efficient planar detector integrated into a deployment-friendly system. The full system design incorporates all the necessary components to construct this state-of-the-art detector system (shown in Figure 11):

- Front-end electronics (including low-noise preamplifiers);
- 84 channels of readout electronics based on extension of the new PHDS SPECT32-HR, including a 12 MeV full range option available by changing a single resistor;
- Power-control board to manage the cooler power, ion pump supply, detector bias supply, preamplifier power, and digital signal processor;
- High resolution camera to provide the accompanying optical overlay;
- A compact, low-power mechanical cooler;
- Two hot-swappable batteries for extended continuous run time away from line power.

Figure 11: The full GeGI-DNN design was completed during Phase I. The GeGI-DNN will be compact and lightweight, with dimensions of 7" diameter and 11.5" long and a weight of 18 lbs.

The overall GeGI-DNN form factor is designed to be lightweight (~18 lbs.) and compact (7" diameter and 11.5" long) with improved battery operation time (2 hours per battery, with onboard connections for 2 batteries). The batteries can be swapped out as many times as desired limited only by the supply of additional batteries. Of significance to this project, the prototype Modular Planar Germanium (MPGe) detector developed for Nuclear Physics was constructed in parallel with this GeGI-DNN Phase-I project. The MPGe design incorporates a 140-mm diameter detector and is relatively lightweight (~32 lbs.) despite no attempt to minimize weight. A similar cryostat design will be used for GeGI-DNN (shown in the expanded image at the bottom of Figure 11), while also investing significant effort to minimize system weight and facilitate ease of internal access (for inspection prior to entry to secure facilities).

The GeGI-DNN design incorporates two significant findings by our LLNL collaborators using the COTS GeGI. Currently, the GeGI includes a 55° C temperature switch that disables the cooler

above this temperature. The GeGI-DNN will use a mechanical cooler that operates smoothly in temperatures up to ~80° C without affecting cooler operation. As such, the temperature cutout switch for GeGI-DNN will be set to 65-70° C to accommodate operation in sunny and hot outdoor environments. Our LLNL collaborators also pointed out a problem with the existing GeGI camera when used in outdoor environments. The GeGI-DNN design incorporates a new high-definition camera that is much more amenable to a variety of operational environments.

In addition to the fundamental GeGI-DNN design, a slip-on pinhole aperture was designed to be easily added to and removed from the GeGI-DNN system when placed on a bench or tripod. A comparison of the COTS GeGI pinhole aperture and the GeGI-DNN pinhole aperture design is shown in Figure 12. In addition, a pinhole plug was designed to accommodate the pinhole open/closed operation (Figure 13).

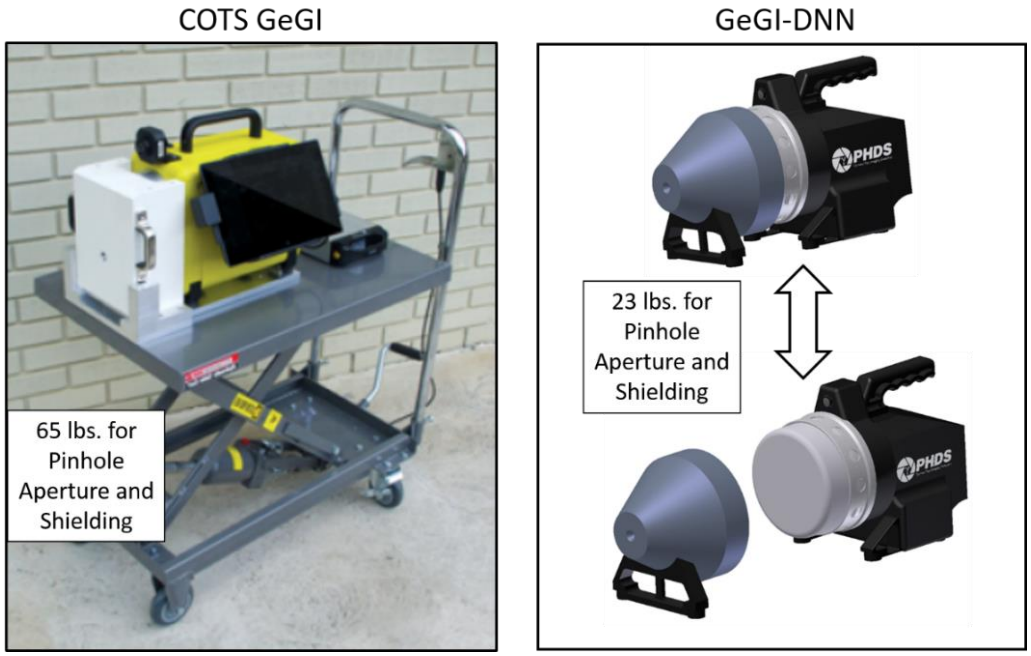

Figure 12: The GeGI-DNN pinhole aperture was designed during Phase I. The pinhole aperture slides over the front of the detector and provides 1" Pb shielding around the pinhole aperture to accommodate imaging special nuclear materials. The COTS GeGI pinhole aperture weighs 65 lbs. and mounts on a cart or heavy duty tripod. The GeGI-DNN pinhole aperture weighs 23 lbs.

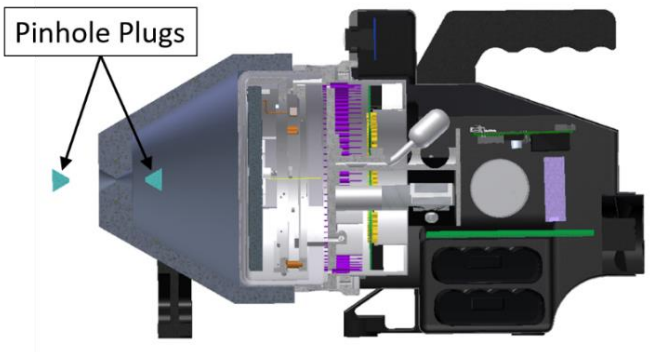

Figure 13: A pinhole plug was also designed for the GeGI-DNN aperture. The pinhole plugs will be joined by a wire and cinched together in the pinhole when the plug configuration is desired.

References

Burks, M., and J. Dreyer. 2014. *GeGI: Chicago field test report (trip #2).* Technical Report, LLNL-TR-656851.

Goulding, Fred S. 1972. "Pulse-shaping in Low-noise Nuclear Amplifiers: A Physical Approach to Noise Analysis." *Nuclear Instruments and Methods* 100: 493.

IAEA. 2015. *Technology Demonstration Workshop on Gamma Imaging: Preliminary External Technical Report.* IAEA Headquarters, Vienna; IAEA Laboratories, Seibersdorf: International Atomic Energy Agency.

Kiser, Matthew, Seth Henshaw, Nathan Hoteling, John Goldsmith, Mark Gerling, Morgan Burks, Jonathan Dreyer, et al. 2014. "Evaluation of Gamma and Neutron Imagers for Radiological/Nuclear Search." OUO Technical Report, DNN R&D.

Pratt, John. 2014. "Gamma Camera Assessment Quick Look." December 9.

Radeka, V. 1968. "State of the art of low-noise amplifiers for semiconductor radiation detectors." *International Symposium on Nuclear Electronics.*

Wahl, Christopher G., Willy R. Kaye, Weiyi Wang, Feng Zhang, Jason M. Jaworski, Alexis King, Y. Andy Boucher, and Zhong He. 2015. "The Polaris-H imaging spectrometer." *Nuclear Instruments and Methods in Physics Research Section A* In Press. doi:10.1016/j.nima.2014.12.110.